Department of Physics and Astronomy
University of Heidelberg

Bachelor Thesis in Physics
submitted by

Deniz Gündüz

born in Villingen (Germany)

2015

Study of the influence of modified light flavour hadron spectra on thermal model hadron densities

This Bachelor Thesis has been carried out by Deniz Gündüz at the

Physikalisches Institut of the University of Heidelberg

under the supervision of

Prof. Dr. Johanna Stachel

Abstract

The influence of the light flavour non-strange baryon mass spectrum on the thermal model descriptions of particle densities in heavy-ion collisions has been studied in this work.

A comparison of densities at a fixed temperature $kT = 156$ MeV and baryochemical potential $\mu_B = 0.1$ MeV shows that modifications of the mass spectrum have a strong effect on the hadron densities. This work shows clearly that a further study in all hadron sectors is vital in order to draw precise conclusions.

Additionally, fits of the model parameters have been done for different mass spectra. The temperature depends weakly on the employed hadron mass spectrum, while the baryochemical potential is not influenced. The results are inconclusive with respect to the improvement of fit quality due to addition of hadron states to the considered spectrum.

Kurzfassung

Der Einfluss des light-flavour-non-strange-Baryonspektrums auf das thermische Modell zur Beschreibung von Teilchendichten in Schwerionenkollisionen wurde in dieser Arbeit untersucht.

Ein Vergleich der Dichten bei einer festen Temperatur $kT = 156$ MeV und einem festen baryochemischen Potential $\mu_B = 0.1$ MeV zeigt einen starken Einfluss von Modifikationen des Massenspektrums auf die Hadrondichten. Diese Arbeit zeigt klar, dass weiterführende Studien in allen Hadronsektoren notwendig sind, um präzisere Schlüsse ziehen zu können.

Zusätzlich wurden Fits der Parameter des thermischen Modells für verschiedene Massenspektren angefertigt. Die Temperatur hängt schwach vom verwendeten Hadronspektrum ab, während das baryochemische Potential nicht beeinflusst wird. Die Ergebnisse ermöglichen keine Rückschlüsse auf die Verbesserung der Fitqualität durch Hinzufügen von Hadronzuständen zu dem betrachteten Spektrum.

Contents

1 Introduction

1.1 Physics at the LHC

On the third of June, 2015, the experiments at the Large Hadron Collider (LHC) took their first physics data after a shutdown of two years. Located at the European Centre for Nuclear Research (CERN), the LHC has been prepared to reach now a centre-of-mass energy of 13 TeV in proton-proton (p–p) collisions. This is close to its design energy of 14 TeV. The previous data taking at 7 TeV and 8 TeV lead to interesting results. With the discovery of a candidate for the Standard Model Higgs boson [1, 2] by the ATLAS[1] and the CMS[2] collaborations, one major goal of the p–p program has been accomplished. It was the last undiscovered component of the Standard Model (SM) of particle physics and has eluded physicists for almost 50 years. Analogous to the Goldstone theorem for global symmetries, the Higgs mechanism gives an explanation for the masses of the Z and $W^{\pm}$ bosons via spontaneous symmetry breaking of the local SU(2)×U(1) symmetry of the electroweak interaction [3]. The fundamental fermion masses can also be explained by interactions with the Higgs field.

Relativistic heavy-ion collisions at the LHC are used to study the many-body physics of the strong interaction. The lead-lead (Pb-Pb) program is dedicated to the study of strongly interacting matter at high temperature. Under these conditions, quantum chromodynamics (QCD), the theory of the strong interaction, predicts a new state of matter, the quark-gluon plasma (QGP). The QGP is characterized by the deconfinement and thermalization of quarks and gluons inside. Studying its signatures and properties is the main goal of the ALICE[3] collaboration. The multipurpose detectors of ATLAS and CMS also participate in the investigation of the QGP.

The measured hadron yields in Pb-Pb collisions at the LHC are well described by the thermal model [4]. This phenomenological model, using statistical mechanics and conservation laws from particle physics, has succeeded over a broad range of energies, from the AGS over RHIC to the LHC [5, 6]. In 2012, however, the ALICE collaboration published a measurement [7] of the p/π ratio for central Pb–Pb collisions at $\sqrt{s_{NN}} = 2.76$ TeV which was lower by about a factor of 1.5 than the models predicted, resulting in a deviation of more than 9σ at the time. Although the deviation has been reduced to about 2.7σ [4], what keeps it interesting is the fact that it concerns protons, very abundantly produced particles in heavy-ion collisions. This "proton puzzle" is one motivation for this work. One crucial in-

---

[1]ATLAS: **A T**oroidal **LHC A**pparatu**S**
[2]CMS: **C**ompact **M**uon **S**olenoid
[3]ALICE: **A L**arge **I**on **C**ollider **E**xperiment

put for the model calculations is the spectrum of considered hadron states. In the following, the influence of a modified hadron spectrum on the behaviour of particle densities and on the parameters of the thermal model is studied. At first, the underlying physics of heavy-ion collisions, the QGP, and the technical aspects of the thermal model are discussed. Afterwards, the numerical implementation of the model is briefly outlined. In the third part, three hadron spectra used in this work and their modifications are presented. Next, hadron densities and ratios of hadron densities for all considered cases are calculated and compared to each other and to ones calculated with the previously employed spectrum. In the last part of the analysis, the model temperature and baryochemical potential are extracted from fits on data from the ALICE collaboration.

1.2 The quark-gluon plasma and heavy-ion collisions

The strong interaction, one of the four fundamental interactions, exhibits two characteristic properties: 'confinement' and 'asymptotic freedom' [8] . 'Confinement' states that the quarks and gluons, the fundamental strongly interacting particles, can never be seen isolated. They are always confined into composite particles, i.e. hadrons. The hadrons can be divided into mesons, bound states of a quark and an anti-quark, and baryons, bound states of three quarks. In order to separate quarks bound in a meson, for example, one needs to spend so much energy that another quark anti-quark pair is formed and the now separated quarks are again parts of two new mesons. 'Asymptotic freedom' describes the behaviour of the strong interaction and short distances or high momentum exchange, which leads to a decrease of the coupling constant α_S. In this situation, it states that quarks and gluons behave like (quasi-)free particles, due to the decreased α_s. Asymptotic freedom could be seen in deep-inelastic lepton-nucleon scattering experiments [9], where quarks were found to be point-like constituent particles of the protons and neutrons.

At very high energies and/or high baryochemical potential μ_B, QCD predicts a phase transition [10] from normal hadronic matter into new forms of matter. Fig. 1.1 shows the assumed phase diagram [11]. One of these new high temperature states is the QGP. It is characterized by the deconfinement of quarks and gluons. In the QGP, they can move freely and are not forced into bound states of hadrons. Another property of the QGP is the chiral symmetry restoration: the quarks acquire their 'current' masses. For the three light quarks, these are much smaller than their 'constituent' masses, which can be assigned to bound quarks. In the case of up- and down-quarks, their current masses of approx. 2 and 5 Mev/c^2 are about 100 times smaller than the constituent masses of about 300 MeV/c^2 [11].

The QGP is assumed to be formed in ultrarelativistic heavy-ion collisions. At the LHC, the Pb-Pb collisions have been measured at a centre-of-mass energy of $\sqrt{s_{NN}} = 2.76$ TeV. There, a 'fireball' of very high energy density is created.
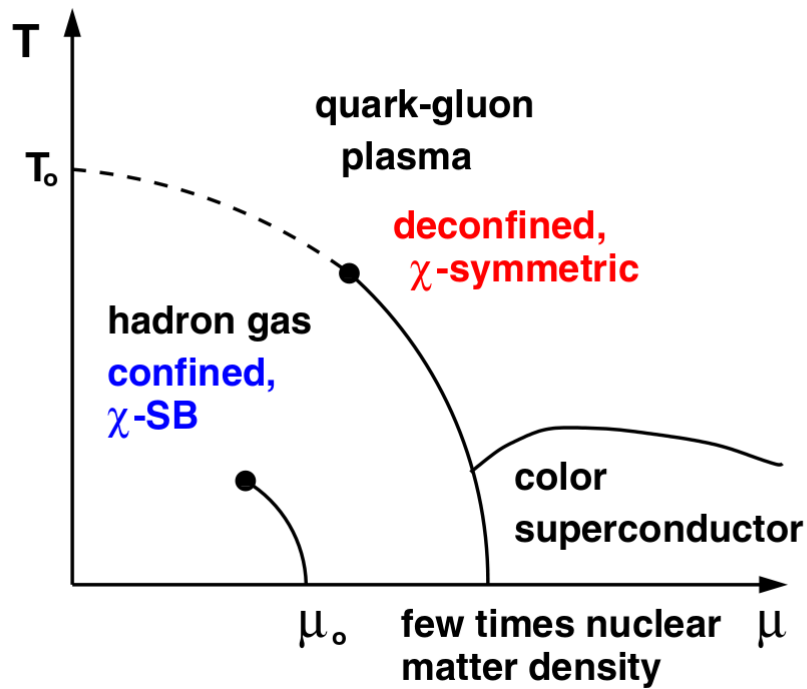
Figure 1.1: Schematical phase diagram of QCD. At low temperatures and low baryochemical potential μ_B, normal hadronic matter resides. Increasing μ_b might lead to a state of colour superconducting matter, while higher temperatures lead to the QGP. The nucleon chemical potential at zero temperature $\mu_0 \approx 938$ MeV, as well as the transition temperature at zero chemical potential T_0 are also shown. Figure taken from[11].

The interactions are assumed to be strong enough to establish a local thermal equilibrium within a very short time (0.1 to 1 fm/c), such that a QGP is formed. This picture is strongly supported by the successful application of hydrodynamics [12].

After the initial collision and the formation, the fireball expands and cools down. At a critical temperature T_c, the system undergoes a phase transition, where confinement is restored and the chiral symmetry is broken. The fireball consists now of many mesons and baryons, which still interact, for a short time, inelastically. The particles are assumed to be in chemical equilibrium at this stage, . Having further cooled down in this time, the particles cease to scatter inelastically at a certain temperature T_{ch}, below which elastic scattering dominates. This process is called 'chemical freeze-out', T_{ch} the 'chemical freeze-out temperature'. After the chemical freeze-out, the hadron abundancies are assumed to not change any longer and the particles are assumed to be in chemical equilibrium. In order to achieve chemical equilibrium after the phase transition, inelastic scattering is necessary. But this interaction becomes less likely since the mean free path increases of the particles due to the decreasing density during the continuing expansion. It has been shown that especially for multistrange particles, high particle densities such as they are present close to the phase transition temperature, are needed [13]. Therefore, kT_c can only be larger than kT_{ch} by a few MeV, with k the Boltzmann constant. After further expansion, elastic scattering processes cease. Now the momenta of the particles are fixed and the hadrons are measured in the detectors. This is called the 'kinetic freeze-out'. It is not yet clear how much time is spent between these two freeze-outs in the hadronic face, or whether there is any time spend at all [14].

It has to be noted that the theoretical approach to the phase diagram faces many difficulties. In four-dimensional Minkowski space, the field equations on QCD cannot be solved analytically. And unlike in quantum electrodynamics, the large coupling constant α_s, which is of the order of unity at low energies, makes perturbative approaches unapplicable. Only at high energies does the value of α_s drop below unity, $\alpha_s(m_z) \approx 0.12$, and power series in α_s may converge. For low energy or long range solutions, QCD on a discretized spacetime lattice, or lattice QCD (LQCD), can be applied as a non-perturbative approach. After calculation of the desired quantities on the lattice, the limit of vanishing lattice spacing has to be taken in order to obtain the physical values. LQCD has shown much promise in predictions of many properties of strongly interacting systems, but is still struggling with calculations at high μ_B or low quark masses. In fact, at LHC energies, the phase diagram of strongly interacting matter is probed at close to vanishing baryochemical potential and high temperature. Lattice QCD calculations at vanishing baryochemical potential indicate that the matter created at the LHC undergoes a rapid smooth crossover from deconfined and chirally restored to hadronic matter [15, 16]. For lower energies and higher baryochemical potential, the phase transition is assumed to be of first order [17].

1.3 Statistical mechanics

The thermal model description of hadron densities in heavy-ion collisions is based on equilibrium thermodynamics. Equilibrium thermodynamics is usually used to describe systems with a large amount of degrees of freedom (d.o.f.) - one litre of gaseous helium for example displays a number of d.o.f of the order of 10^{22}. By giving up the knowledge about every single d.o.f., i.e. the microstate of the system, and rather focussing on a few characteristic parameters, i.e. the macrostate, one can calculate and predict properties of thermodynamic systems much easier than solving the associated differential equations for every d.o.f. seperately. This ensemble theory has shown itself to be very powerful in describing systems with many d.o.f. by going over to so-called ensemble values. These quantities are for example the energy of the system, the volume, its entropy or temperature.

Besides the high number of d.o.f., standard thermodynamics needs the concept of equilibrium to work properly. A system is in equilibrium if its ensemble averages do not change in time any more. Only in equilibrium are the above-mentioned quantities properly defined and usable. The theoretical understanding of equilibration in heavy-ion collisions is still not complete and under discussion.

There are three different types of ensembles: microcanonical, canonical, and grand canonical. The construction of these ensembles is based on extremizing the entropy while at the same time obeying the constraints of known properties of the systems. In a microcanonical ensemble, the energy E, its volume V and the number of particles N are exactly known. Every microstate that leads to this macrostate can be found with the same probability. Thus, these three quantities are sufficient to describe our system.

In a canonical ensemble, exchange of energy with the environment is allowed, therefore the knowledge of E is not exact any more. Only the average energy is known. To extremize the entropy with this constraint, one can introduce a Lagrange multiplier β. This object is connected to the physical temperature T by $\beta = \frac{1}{kT}$, with the Boltzmann constant k. Instead of the energy, one can now describe the system with T, V, and N.

The grand canonical ensemble is characterized by the exchange of heat and particles. So now one needs to introduce a second Lagrange multiplier to obey the constraints on E and N. It turns out that a convenient choice for this multiplier is $\beta \cdot \mu$, with μ the so-called chemical potential. The chemical potential μ, which has the dimension of an energy, can be thought of as the cost of energy to add one particle to the system. If more than one type of particles are present, one needs to introduce a chemical potential μ_i for each type. For this type of system, the characteristic parameters are T, V, and all μ_i.

In the following model, the grand canonical formulation is used to describe thermodynamic properties of the medium created in heavy-ion collisions. With one adjustment: When looking at a relativistic system of strongly interacting particles, the (not conserved) total number of particles is replaced by the conserved quantities, namely one component of isospin, baryon number, strangeness and charm. Therefore, we have four chemical potentials, one for each of these quan-

tum numbers.

For thermodynamic calculations, the partition function is a very useful quantity. In the grand canonical ensemble, the partition function $\mathcal{Z}$ of an ideal relativistic quantum gas in terms of the canonical partition function Z is given by:

$$\mathcal{Z}(T, V, \mu) = \sum_{N=0}^{\infty} e^{\beta \mu N} Z(T, V, N) \tag{1.1}$$

$$= \sum_{N=0}^{\infty} e^{\beta \mu N} Tr[e^{-\beta H}] \tag{1.2}$$

$$= \sum_{[k_l]} e^{-\beta \sum_l (\epsilon_l - \mu) k_l} = \prod_l \sum_{k_l} e^{-\beta(\epsilon_l - \mu)k_l} \tag{1.3}$$

$$= \begin{cases} \prod_l \frac{1}{1 - e^{-\beta(\epsilon_l - \mu)}}, & \text{for bosons,} \\ \prod_l (1 + e^{-\beta(\epsilon_l - \mu)}), & \text{for fermions,} \end{cases} \tag{1.4}$$

where H is the Hamiltonian of the system, $\epsilon_l = \sqrt{(p_l c)^2 + (mc^2)^2}$ its l-th eigenvalue, k_l the occupation number of the l-th state, and $[k_l]$ one possible combination of occupation numbers. Again, one has to bear in mind that the N in this formula is not necessarily the particle number, but rather a representative conserved quantity. In order to regain the status of particle number, one can define a chemical potential for each species in the following way:

$$\mu_i = \mu_B B_i + \mu_{I_3} I_{3i} + \mu_S S_i + \mu_C C_i \tag{1.5}$$

with the baryon number B_i, the third component of isospin I_{3i}, the strangeness S_i and the charm C_i of the particle species i, and the corresponding chemical potentials μ_B, μ_{I_3}, μ_S and μ_C. To calculate for example the number density n_i of particle species i, one can make use of the Laundau- or grand potential Φ_G:

$$\Phi_G(T, V, \mu) = E - TS - \mu N = -PV = -\frac{1}{\beta} \ln \mathcal{Z} \tag{1.6}$$

with the entropy S and the pressure P. In the thermodynamic limit of infinitely large volume, one can write:

$$\lim_{V \to \infty} \ln \mathcal{Z}_i = \lim_{V \to \infty} \sum_l \pm \ln(1 \pm e^{-\beta(\epsilon_l - \mu_i)}) \tag{1.7}$$

$$= \lim_{V \to \infty} g_i \sum_p \pm \ln(1 \pm e^{-\beta(\epsilon(p) - \mu_i)}) \tag{1.8}$$

$$= \lim_{V \to \infty} g_i \frac{1}{\Delta} \sum_p \pm \Delta \ln(1 \pm e^{-\beta(\epsilon(p) - \mu_i)}) \tag{1.9}$$

$$= \pm g_i \frac{V}{(2\pi\hbar)^3} \int d^3 p \ln(1 \pm e^{-\beta(\epsilon(p) - \mu_i)}) \tag{1.10}$$

$$= \pm g_i \frac{V}{2\pi^2 \hbar^3} \int_0^{\infty} dp \, p^2 \ln(1 \pm e^{-\beta(\epsilon(p) - \mu_i)}), \tag{1.11}$$

with g_i being the spin degeneracy factor and $\Delta = (\frac{2\pi\hbar}{L})^3$ the position-space volume element for a given discrete momentum p. The positive sign applies to fermions, the negative one to bosons respectively. Now, for the density n_i, we get:

$$n_i = -\frac{1}{V}\left(\frac{\partial\Phi_G}{\partial\mu_i}\right)_{V,T=const} = \frac{g_i}{2\pi^2\hbar^3}\int\limits_0^\infty \mathrm{d}p \, \frac{p^2}{e^{\beta(\epsilon(p)-\mu_i)}\pm 1} \qquad (1.12)$$

A more detailed description of thermodynamics can be found in [18].

The number of produced hadrons in central Pb-Pb collisions may be of the order of ten thousand, but still small compared to other thermodynamical systems. Because of the small size of the system, the canonical approach for the strangeness is deemed more accurate. The difference between these two approaches is given by the implementation of the conservation laws. In the canonical ensemble, the conservation laws must be obeyed locally and they have to be implemented on an event-by-event basis. This leads to a major reduction of phase space for strange particles compared to the grand canonical approach, where conservation laws have to be obeyed on average. This difference is known as canonical suppression of strangeness. It has been shown, however, that the difference between calculated hadron densities in these two approaches depends on the number of participants in the collisions N_{part} and the centre-of-mass energy. For a high number of participants, the two formulations yield almost equal hadron densities. For example, at top SPS energies, deviations of about 10% can be seen for moderately central Pb-Pb collisions, corresponding to $N_{part} \approx 100$. Therefore, the grand canonical ensemble can be used accurately to describe at least central collisions with a a large number of participants at high energies [19].

1.4 The Hagedorn spectrum

An important theoretical approach to the phase transition of strongly interacting matter is the Statistical Bootstrap Model (SBM) developed by Hagedorn in the 1960s [20]. In this model, the produced fireball is said to consist of smaller fireballs, which consist of smaller fireballs themselves. This is known as the 'Bootstrap Condition'. Hagedorn predicted, at least for large masses, an exponentially growing mass spectrum $\rho(m)$ for hadrons,

$$\rho(m) \propto \frac{1}{m^a}e^{m/T_0} \qquad (1.13)$$

with a characteristic temperature T_0 and a model parameter a [20]. In the SBM, the partition function $Z(T,V)$ features a singularity at T_0, giving rise to the interpretation of a limiting temperature for hadronic matter. The nature of the singularity is given by the parameter a. The hadron spectrum in the 1960s lead to the values $kT_0 = 160$ MeV and $a = \frac{5}{2}$, displaying an exponential character which hasn't been realised before. Hagedorn's choice for a also lead to a singularity in the energy density at $T = T_0$, reinforcing the limiting character of T_0.

For a larger value of a, namely $a > \frac{7}{2}$, however, a finite value for the energy

density could be achieved, making the transition into a phase possible where a new description of matter would be needed. Today, this temperature is assumed to be the critical temperature for the phase transition from hadronic matter to the QGP.

2 Implementation of the thermal model

As illustrated in Section 1.3, the thermodynamics of heavy-ion collisions can be described in the grand canonical formalism by six parameters. Four of these parameters can be fixed by conservation laws.
The volume can be determined from the conservation of baryon number:

$$V \sum_i n_i B_i = Z + N \tag{2.1}$$

with the number of protons Z and the number of neutrons N that participate in the collision. Next, the strangeness and charm chemical potentials μ_S and μ_C are determined by their respective conservations, leading to following conditions:

$$\sum_i n_i(\mu_s) S_i = 0 \tag{2.2}$$

$$\sum_i n_i(\mu_C) C_i = 0 \tag{2.3}$$

At last, the conservation of the third component of isospin I_3 fixes μ_{I_3}:

$$V \sum_i n_i(\mu_{I_3}) I_{3i} = \frac{Z - N}{2} \tag{2.4}$$

, leaving a total of two free model parameters: the temperature at the chemical freeze-out T_{ch} and the baryochemical potential μ_B. For a more accurate description, interactions between particles have to be introduced to the equations of section 1.3. It has been argued that the attractive interactions can be implemented by counting the resonance states of every particle separately as a particle of its own [21]. For the repulsive interactions, the code features an eigenvolume correction after Rischke, Gorenstein, Stöcker and Greiner [22, 23]. The particles are assumed to be hard spheres of a certain radius R and are not allowed to come closer than a distance of $2R$. This resembles the Van-der-Waals correction for classical ideal gases. A common radius for mesons and baryons of $R = 0.3$ fm is currently applied. The corrected density formula is now given by:

$$n_i^{excl}(T, \mu_1, ..., \mu_m) = \frac{n_i(T, \hat{\mu}_i)}{1 + \sum_j v_{0,j} n_j(T, \hat{\mu}_j)} \tag{2.5}$$

where $\hat{\mu}_i$ is given by

$$\hat{\mu}_i = \mu_i - v_{0,i} P^{excl}(T, \mu_1, ..., \mu_m) \tag{2.6}$$

with the pressure P^{excl} and $v_{0,i}$ the eigenvolume of the hadron. The thermal code calculates the thermodynamic properties and provides data, which can be compared and fitted to experimental data and can be even used for predictions. It uses the following procedure: As a first step, the initial[1] (primordial) hadron densities given by equation 2.5, the total charm, strangeness, and third component of isospin are calculated for a given temperature and baryochemical potential. Next, in form of several successive loops, the conservation laws[2] are checked and, if not fulfilled, the associated chemical potential is corrected. After correction, the code runs again from the innermost loop until the deviations become small enough compared to the output. Following these loops, the entropy and energy density are calculated. As a last step, the densities after particle decays mediated by the strong and weak interaction (strong and weak decays) are calculated.

One crucial part of the thermal code is the listing of considered hadron species. It contains all necessary information about the hadrons, from mass over degeneracy g due to total angular momentum J to branching ratios of its decay channels. As of the beginning of 2015, 223 mesonic and 324 baryonic states were included. This includes 123 nonstrange mesons, 32 strange ones, 40 charmed mesons and 28 bottom mesons. On the baryon side, 48 nonstrange baryons, 48 strange ones, 56 charmed and 14 bottom baryons. Light nuclei such as deuteron or triton, combinations of mesons and baryons, and even hypernuclei, nuclei containing hyperons, are also listed as possible collision products. These states and their antiparticles account for 62 entries. Table 2.1 shows an example of such a state with the information provided by the list. The width stands for the Breit-Wigner width of the resonance state. The threshold denotes the lower boundary of the distribution. Both are used in corrections of the densities [24], which are negligible at LHC energies. The number of possible decay products is denoted in the seventh column, the products themselves listed as decay modes in the eight one. In the next column, the probabilities for these particles to result from decays are listed. As the code computes the hadron densities after all strong and weak decays, the individual branching ratios of the decay channels can be added up to get the cumulative probability of a particle to be produced in the decay of the resonance. The code does not distinguish between the different decay channels, as one is only interested in the final overall densities for each species.

Apart from interactions, the measured hadron yields include also the particles coming from decays of higher mass states. To account for these, information on the decay properties of each individual state is needed. The implementation of the decay chains is another important part of the code. In the beginning, the code creates a quadratic array R_{mn}, whose diagonal entries are given by the primordial densities of every state listed in the hadron spectrum. The densities are calculated as in equation (2.5). This array stores all hadrons of every sort ever seen in the detector. In the beginning, the code creates a quadratic array R_{mn}, whose diagonal entries are given by the primordial densities of every state listed in the spectrum. The densities are calculated as mentioned above. This array will

---

[1] initial meaning before any decays
[2] still no equations in theory part

Resonance	g	Mass in MeV	Width/Threshold in MeV	I_3	charge in e	# decmod	decay modes	decay prob.
p	2	938.3		$+1/2$	$+1$	0		
n	2	939.6		$-1/2$	0	0		
p(1440)	2	1440	300 / 1073	$+1/2$	$+1$	8	n	0.483
							p	0.267
							π^+	0.542
							π^0	0.417
							π^-	0.142
							Δ^{++}	0.125
							Δ^+	0.083
							Δ^0	0.042
n(1440)	2	1440	300 / 1075	$-1/2$	0	8	n	0.267
							p	0.483
							π^-	0.542
							π^0	0.417
							π^+	0.142
							Δ^-	0.125
							Δ^0	0.083
							Δ^+	0.042

Table 2.1: Example of 3 hadron states with the information found in the list. Detailed explanation of the entries can be found in the second paragraph of this section.

later store all particles of every sort which are either present in the final state or which are at least potentially reconstructable from the final state particles. Next, the decay array D_{mn}, is worked out. Its entries give the probability of state m to decay into state n. To now get the resulting densities, one needs to do repetitive matrix multiplications. The very first two iterations are as follows: The code fills a decay vector d_h with the results of the first decay, i.e.

$$d_h = D_{mh} \cdot R_{mm}, \tag{2.7}$$

which is then added to the result array,

$$R_{mh}^{after} = R_{mh}^{before} + d_h, \tag{2.8}$$

filling the m-th row with the densities of the decay products h. The next step is composed of calculating the result vector r_j,

$$r_j = D_{hj} \cdot d_h, \tag{2.9}$$

which is just another matrix multiplication with the decay array. This result vector contains the densities after a second round of decays and is also added to the result array in the same manner as in equation (2.8). And by now making the result vector the new decay vector, an iterative algorithm is defined that lets all states decay until there is nothing unstable left.

3 Modifications of the Hadron List

3.1 Hadron spectra

As discussed above in formula (1.1), the partition function of the system and therefore the calculation of particle densities, depend on the spectrum of permitted states k_l. The newest experimental results on the hadron spectrum and particle physics in general are collected by the Particle Data Group (PDG) and published biennially. The hadron states are rated after the quality and quantity of evidence for their existence, ranging from poor (*) to certain(****) evidence for existance. This work will be based on the most recent version [25] from 2014. In this chapter, three different mass spectra to be used later in the calculations are presented. These spectra will differ in their respective N and Δ resonance sectors.

The N and Δ resonance states consist of u- and d-quarks. They differ in their total isospin: the N states have a total isospin of $I = \frac{1}{2}$, the Δ states have $I = \frac{3}{2}$. As the lightest baryons, when keeping the quantum numbers constant, they are produced more abundantly than the heavier ones in heavy-ion collisions. There are several problems with the identification of these resonances. As one can see in Fig. 3.1, the total $p\pi$ cross section shows one distinctive peak at $\sqrt{s} \approx 1200$ GeV, corresponding to the $\Delta(1232)$ resonance and three smaller peaks at $\sqrt{s} \approx 1700$, 2000 and 2500 GeV can be seen. Other distinctive features are not present. The extraction of the resonant Δ states is difficult due to the broadness of each of these resonances and the shadowing of smaller peaks by the $\Delta(1232)$. This problem could be solved by improved statistics. With enough data, eventually all peaks and their corresponding resonance states could be identified. What hinders the extraction more is the interference of these states: As they all are produced in the same process with the same initial and final state, $N\pi \to N^*$ or $\Delta^* \to N\pi$, the total cross section is proportional the absolute square of the sum of each amplitude,

$$\sigma_{tot} \propto |\sum_i \mathcal{M}_i|^2 \tag{3.1}$$

where i denotes the resonances. This leads to many interference terms which make the identification highly non-trivial. The experimental method to extract the non-strange light flavour resonance states from cross sections is a partial wave analysis. Here, the amplitudes $\mathcal{M}$ are expanded in partial waves. There are different ways and different approximations used by the various groups, leading to a variation of spectra for the N and Δ states.

In the following, the three considered spectra are discussed in more detail.
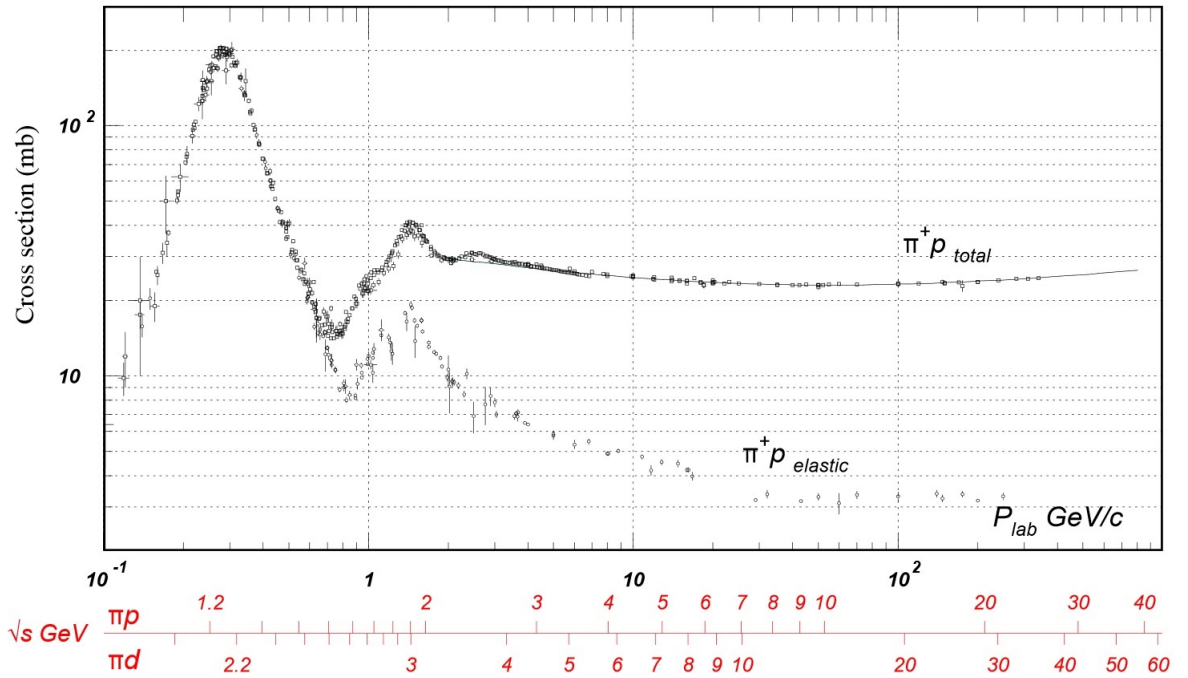
Figure 3.1: Total and elastic $p\pi^+$ cross section. Most prominent feature is the $\Delta(1232)$ peak. Plot taken from [25].

GWU-modified PDG 2014

The first particle spectrum is a variation of the PDG 2014 hadron list. This spectrum takes the recent partial wave analysis from the George Washington University (GWU) into consideration, meaning that only states that have reasonable evidence for their existence and that were found by the GWU analysis are considered and implemented in the code. The PDG states this analysis as the most recent and most complete. Reasonable evidence is assumed to be given by a rating of (**). This spectrum contains a total of 20 N states (including proton and neutron) and 10 Δ states. Compared to the version of 2008, 8 nucleon and 9 Δ resonances are removed from the list of considered states, whereas only 5 N states are added, leading in total to a reduction of the overall number of possible resonances.

PDG 2014 unmodified

The next spectrum is an unmodified version of the non-strange light-flavour resonance listing put together by the PDG as of 2014. In this version, all states with a rating of (**) or higher are considered as possible states and therefore listed in the code, even if they were not found by the GWU analysis. This second version adds 8 Ns and 1 Δ compared to the spectrum from the 2008 edition, while only

N states	Δ states
p,n	
N(1440)	Δ(1232)
N(1520)	Δ(1600)
N(1535)	Δ(1620)
N(1650)	Δ(1700)
N(1675)	Δ(1905)
N(1680)	Δ(1910)
N(1720)	Δ(1930)
N(1860)	Δ(1950)
N(1880)	Δ(2400)
N(2000)	Δ(2420)
N(2040)	
N(2120)	
N(2190)	
N(2220)	
N(2250)	
N(2300)	
N(2570)	
N(2600)	

Table 3.1: List of light flavour nonstrange baryon states in the GWU-modified PDG 2014 spectrum

N states	Δ states
N(1700)	Δ(1900)
N(1710)	Δ(1920)
N(1875)	Δ(1940)
N(1895)	Δ(2000)
N(1900)	Δ(2150)
N(1990)	Δ(2200)
N(2700)	Δ(2300)
	Δ(2350)
	Δ(2390)
	Δ(2750)
	Δ(2950)

Table 3.2: List of additional states in the unmodified PDG 2014 hadron spectrum.

removing 2 of the nucleon resonances.

PDG 2014 with LQCD spectrum

The third spectrum includes the unmodified PDG 2014 resonances as well as states that have been taken from LQCD calculations [26]. The baryon excitations have been calculated at a pion mass of $m_\pi = 396$ MeV/c^2. The full spectrum can be seen in Fig 3.2. In order to obtain the masses of the excited states at the physical pion mass of about 140 MeV/c^2, the following scaling procedure is applied: At first, the masses of the different states are extracted from Fig. 3.2. Afterwards, the known resonances are identified in the lattice spectrum through their masses, the mass ordering, total angular momentum and parity. The average difference between the lattice masses and the ones in the PDG for the identified states are of the order of 10% for both N and Δ resonances. Then, for these resonances, the mass ratio between LQCD and PDG is calculated as an individual scaling factor f_i. Next, the average of the f_i is determined in order to obtain an overall scaling factor f. This procedure is separately applied for the N and Δ states. For the Ns, the scaling factor $f_N \approx 0.7088$ and for the Δs the factor $f_\Delta \approx 0.7600$ has been calculated. The maximum deviation $\delta_{f,max}$ between individual and average factors is approximately $\frac{\delta_{f_N,max}}{f_N} = 15\%$ for the N states and $\frac{\delta_{f_\Delta,max}}{f_\Delta} = 18\%$ for the Δ resonances. Afterwards, these scaling factors are applied to the masses obtained from [26].
This spectrum contains 23 additional N and 10 additional Δ resonances compared to the version PDG 2014 version.
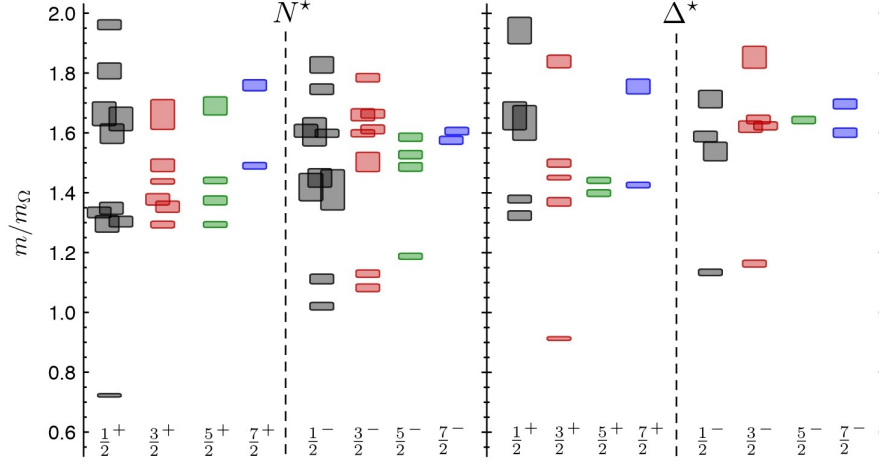
Figure 3.2: Light flavour non-strange baryon spectrum calculated from lattice QCD. The total spin of the states is given on the x-axis. The y-axis shows the mass of the states in multiples of the Ω mass calculated on the same lattice, in order to remove explicit scale dependence. Fig. taken from [26]

N states	N states	Δ states
N(1200)	N(1779)	Δ(1690)
N(1290)	N(1813)	Δ(1700)
N(1315)	N(1849)	Δ(1766)
N(1529)	N(1896)	Δ(1780)
N(1552)	N(1908)	Δ(1931)
N(1588)	N(1909)	Δ(2033)
N(1600)	N(1920)	Δ(2059)
N(1612)	N(1967)	Δ(2097)
N(1623)	N(1973)	Δ(2135)
N(1635)	N(2074)	Δ(2364)
N(1683)	N(2169)	Δ(2465)
N(1778)		

Table 3.3: List of additional states calculated from LQCD.

3.2 Decay properties

The implementation of new resonance states into the hadron spectrum requires information about the decay properties of the corresponding states. If the measured branching ratios differ by less than 20% between the different analyses quoted by the PDG, the central value is taken. If measurements differ by more or no branching ratios are stated, the decays are constructed in analogy to states with similar masses and angular momentum. The masses are deemed similar if the deviation is less or equal to 100 MeV/c^2. In the case that there are no similar states, the properties are calculated by hand with the assumption that only kinematically allowed two-body decays occur. Then, the partial branching Γ is given by [25]:

$$\mathrm{d}\Gamma = \frac{1}{32\pi^2}|\mathcal{M}|^2\frac{|\boldsymbol{p}_1|}{M^2}\mathrm{d}\Omega \tag{3.2}$$

with $\mathcal{M}$ the decay matrix element, M the mass of the mother particle, $\boldsymbol{p}_1$ the momentum, and $\mathrm{d}\Omega$ the solid angle of one daughter particle. The momentum is given by:

$$|\boldsymbol{p}_1| = \frac{[(M^2 - (m_1 + m_2)^2)(M^2 - (m_1 - m_2)^2)]^{\frac{1}{2}}}{2M} \tag{3.3}$$

where $m_{1,2}$ stands for the masses of the daughter particles. To get an estimate for the quality of this approximation, the partial branchings for established states have also been calculated in this manner. Again, the difference between the PDG values and the approximation are of the order of 10%. For example, the PDG states for the decay channel $N(1520) \to N\pi$ a branching ratio of $\approx 60\%$, whereas the calculated branching ratio is $\approx 54\%$.

4 Results

The presentation of the results will be split in three parts. In the first part, using the thermal model, hadron yields for Au-Au-collisions are computed for a temperature of $kT = 156$ MeV and a baryochemical potential of $\mu_B = 0.1$ MeV. The value for the temperature is the same as the one obtained by the most recent fit on LHC data [4]. The difference in μ_B is negligible. The densities are calculated for the three spectra and then compared to the previous hadron spectrum, last revised in 2008, and to each other.

In the second part, the calculated yields are fitted to LHC data for Pb-Pb collisions in order to extract values for T and μ_B. The last part shows a comparison of the three spectra with Hagedorn mass spectra for different critical temperatures.

4.1 Densities and ratios at fixed temperature

The GWU-modified PDG 2014 hadron spectrum lists less baryon resonances than the already implemented one. This leads to a minor increase of initially produced hadrons at a fixed temperature compared to the old version. This increase can be explained by the eigenvolume correction. Equation 2.5 shows that the removal of states which would contribute to the sum in the denominator leads to an increase in density. The hadron yields after strong decays show a different trend. The proton and neutron densities decrease by about 3.2%. The pion densities decrease also, but only by a factor of 0.4%. The density ratios for a variety of hadrons can be seen in Fig. 4.1. The decrease in the proton and neutron, as well as in the pion and the Δ resonance densities can be explained by the missing resonances which would decay into these particles.

The unmodified PDG 2014 mass spectrum consists of more hadronic states than in 2008. Hence, one can observe the contrary effect for the primordial hadron yields. As more hadron states are included in the list, more terms contribute to the sum in the eigenvolume correction, leading to a decrease of initial particle densities. But now there are more possible baryon states than before and the calculations show that the production of baryons is slightly favoured over the meson sector. The net baryon number stays the same, it is conserved in the collision, but the total number of baryons, i.e. the number of baryons and antibaryons, shows an increase.

This increase leads to a complementary situation after the strong decays to the one above, which can be seen in Fig. 4.2. The additional resonances decay mostly into nucleons and pions, and their densities show an increase of about 2.3% for the proton and neutron, and 0.2% for the charged pions. The primordial densities of the added resonances can account for this effect, resulting in additional
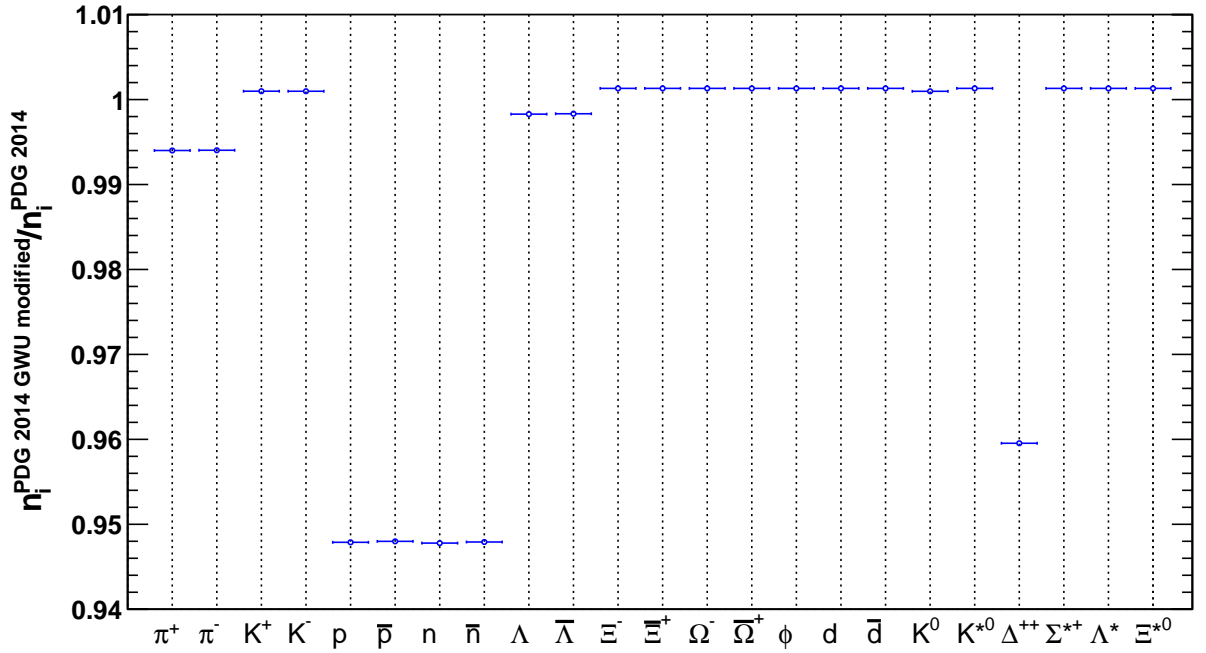
Figure 4.1: Ratio of hadron densities. In this plot, the ratio is given by the densities calculated with the GWU-modified version of the PDG 2014 versus the unmodified PDG 2014 version.
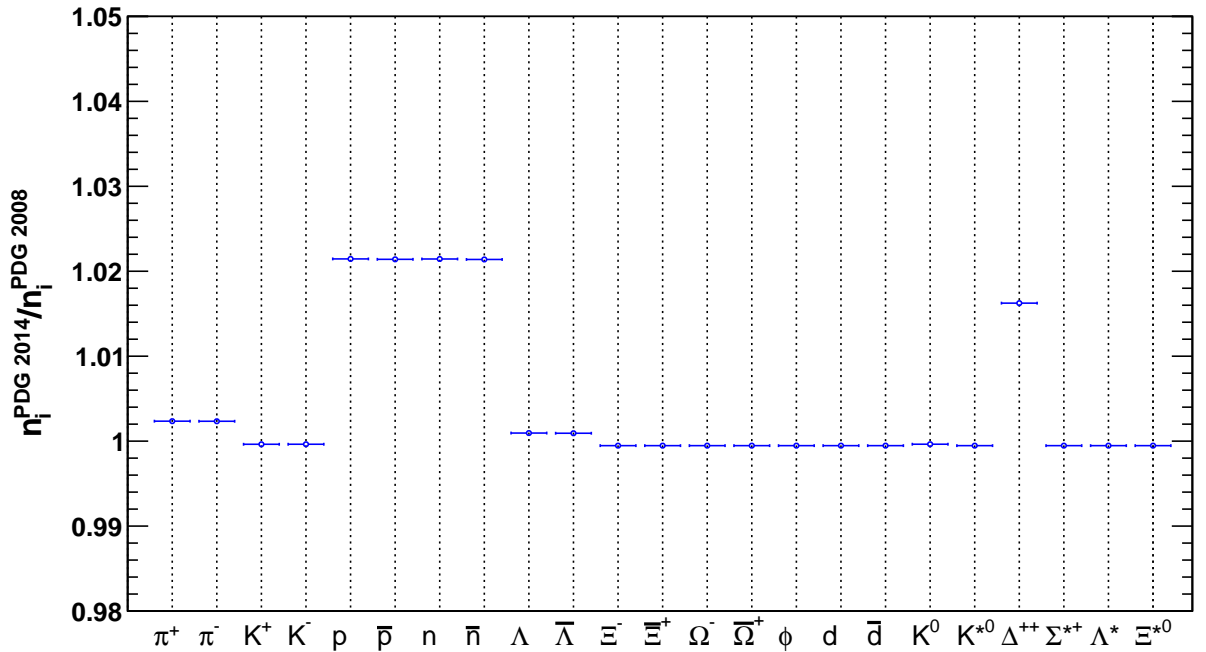

Figure 4.2: Ratios of the unmodified PDG 2014 version versus the PDG 2008 mass spectrum
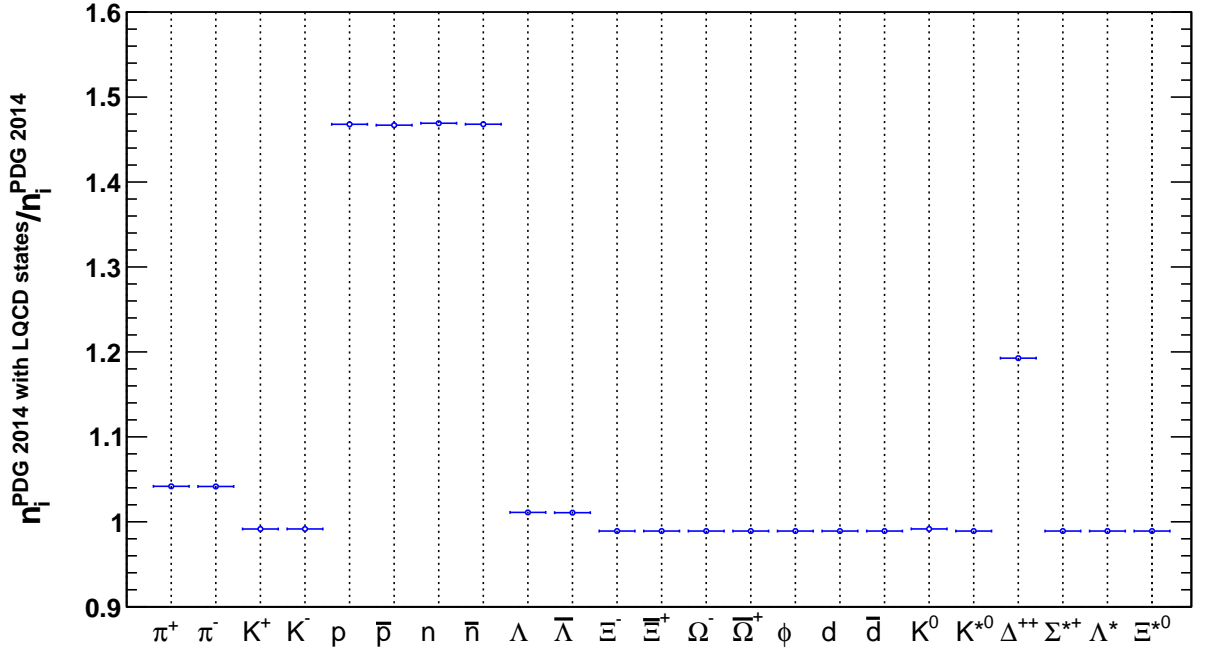
20

Figure 4.3: Comparison of the PDG 2014 with LQCD mass spectrum to the un-
modified PDG 2014 hadron list

feed-down protons, neutrons and pions.

The third spectrum, the LQCD motivated one, qualitatively shows the same trends as the unmodified PDG 2014 case. Quantitatively, given the many additions seen in Table 3.3, a rise in protons of about 49.9% and in neutrons of about 50.1% has been calculated. The charged pions again show a rise of about one tenth of the nucleons, roughly 4.4%. The discrepancy between the pion and the nucleon boost can be explained by the fact that most pions come from meson decay and initial production. Comparison of the absolute densities show a greater absolute increase in pions than in nucleons, but the amount of pions from mesonic decays is much greater, leading to the smaller relative gain. Fig. 4.3 shows the ratios of the LQCD spectrum yields versus the yields from the second spectrum. The small boost of Λ baryons and the significant rise in Δ baryons can again be explained by the decay channels of the higher mass nucleon and Δ states.

4.2 Fit on LHC data

The yields are fitted to data from the ALICE experiment at the LHC. The fit routine is based on a χ^2 minimization. The uncertainties considered in the fit are the experimental uncertainties of the hadron yields. Fig. 4.4 shows the experimental values of particle yields for the 10% most central Pb-Pb collisions at a centre-of-mass energy of $\sqrt{s} = 2.76$ TeV and the fit of the statistical model yields for the first scenario. The fit in this case leads to a temperature of $kT = 157$ MeV
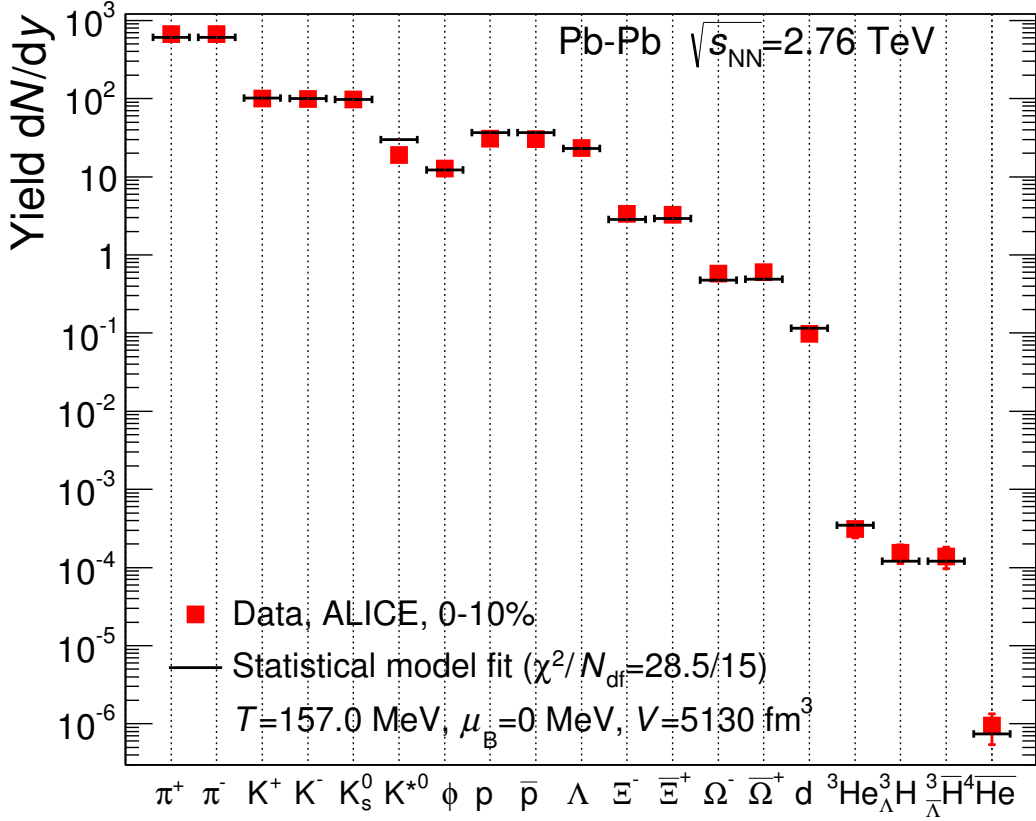
Figure 4.4: Extraction of T_{ch} and μ_B from fit on yields for the GWU-modified PDG 2014 spectrum.

and a chemical potential of $\mu_B = 0$ MeV. The same values are obtained in the most recent published fit of the LHC parameters [4]. The GWU modified spectrum leads to a slightly improved fit qualitiy, the $\chi^2/d.o.f.$ reduces from $34.4/15$ to $28.3/15$. The proton and antiproton yields still deviate by more than 2.5σ (cf. fig. 4.5), but except from the K^*, which has not been considered for the fit, the predicted yields and the measured ones agree.

The fit results for the full PDG 2014 hadron list is shown in Fig. 4.6. This spectrum, containing several more states, leads to a very similar temperature of $kT = 156$ MeV and a vanishing baryochemical potential. But the quality of the fit degrades, the $\chi^2/d.o.f.$ rises from $34.4/15$ to $37.4/15$. The deviations between predicted and measured yields grow, the values for proton and antiproton are now almost 3σ apart. The model shows a trend of overestimating the nucleon densities while underestimating the strange particle yields. Fig. 4.8 shows the fits for the lattice spectrum. The temperature drops to $kT = 150$ MeV, and $\mu_B = 0$ MeV. The quality of the fit degrades further, the $\chi^2/d.o.f. = 160.5/15$ is significantly higher than in the other cases. Proton deviation now reach a significant value of above 3σ. The overestimation of proton yields is now much larger. The other species are also more strongly underestimated, except for the K^*, which leads to
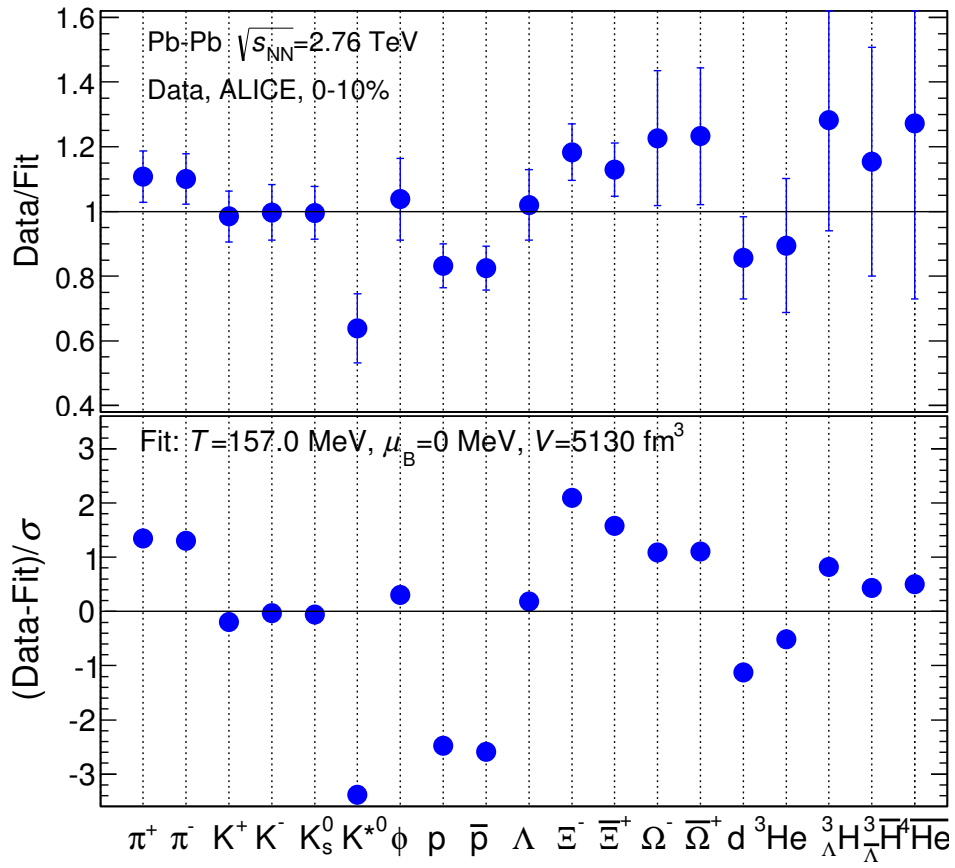
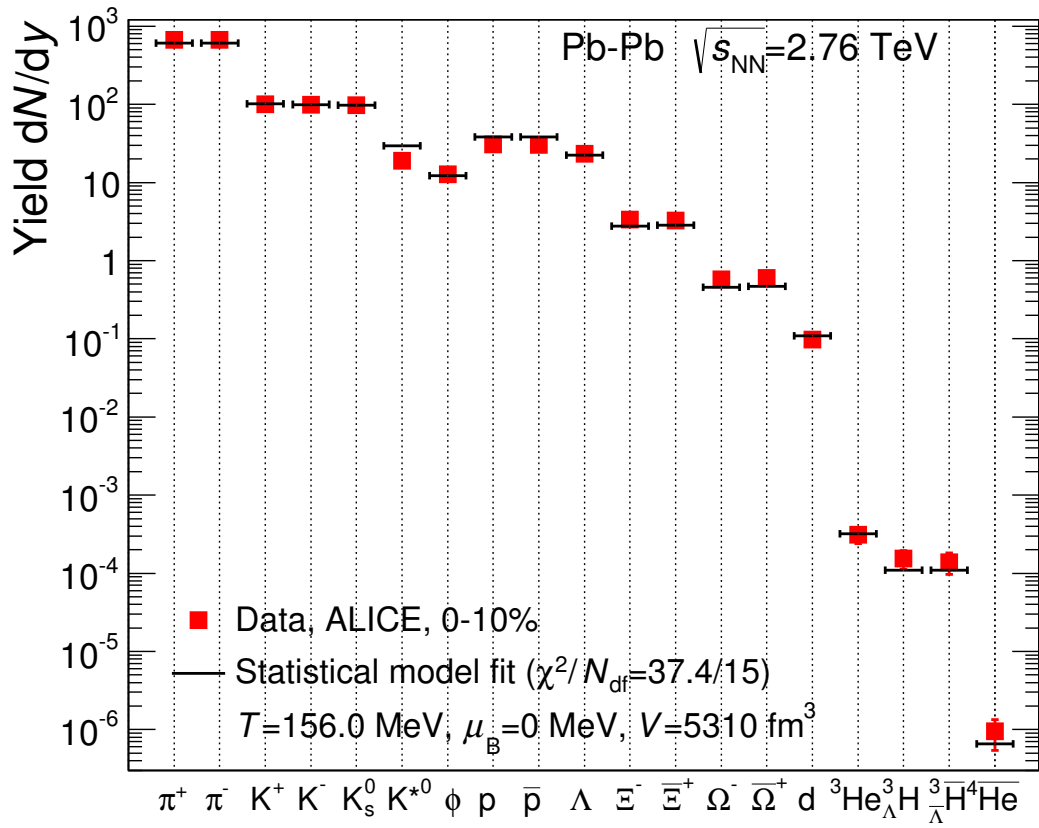Figure 4.5: Differences between data and fit for the GWU-modified PDG 2014 spectrum.

Figure 4.6: Extraction of T_{ch} and μ_B from fit on yields for the unmodified PDG 2014 hadron list.
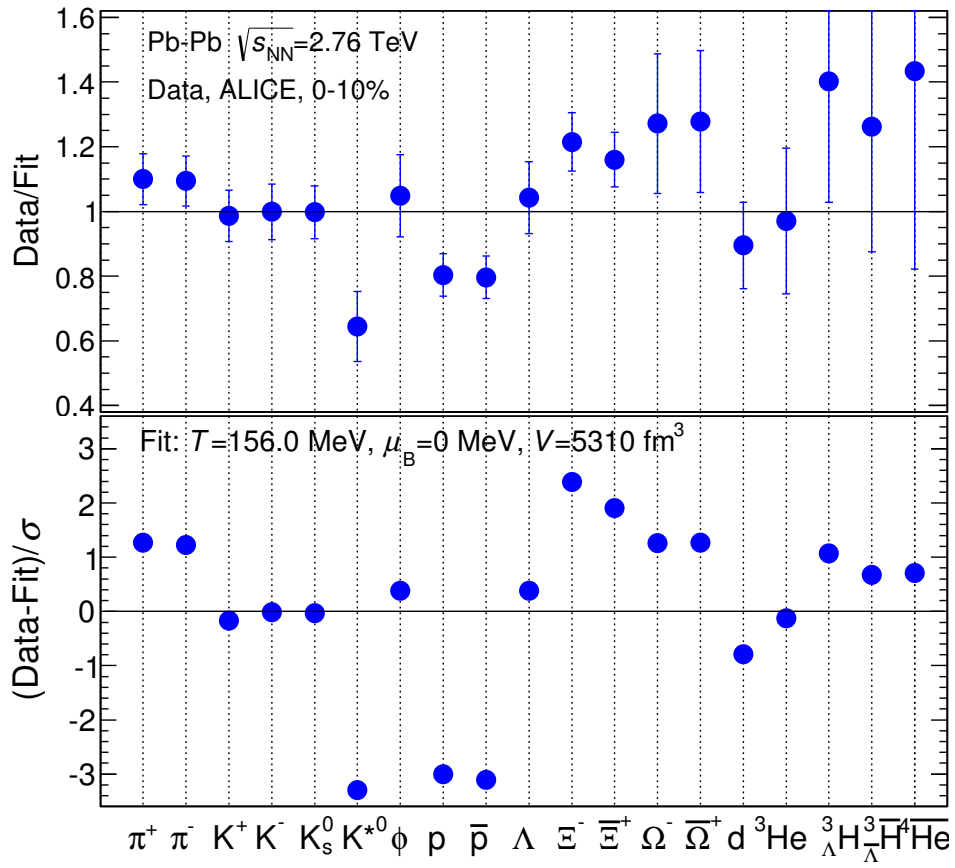
Figure 4.7: Differences between data and fit for the unmodified PDG 2014 hadron list.

the deterioration of the $\chi^2/d.o.f.$. Despite the large differences in the spectrum and the worse fit quality, the temperature does not drop as much as one could have expected. If one were to not consider the protons in the fit, the largest deviation would be given by the cascades $\Xi^\pm$,which differ by approximately 5σ. For the other species, the thermal model yields and the measured ones still roughly agree. Excluding the protons might therefore lead to a slightly improved fit quality.

The baryochemical potential is not influenced by the hadron spectrum. It depends on the ratio between baryons and antibaryons, which is not affected by the number of different species of baryons considered in the spectrum. In the Boltzmann limit, where quantum statistics are neglected, μ_B is given by

$$\mu_B = \frac{1}{2B_i} \ln \frac{\bar{n}_i}{n_i} \tag{4.1}$$

with the baryon number B_i and the density n_i for a non-strange light flavour baryon. Apart from the pions, this is a rather good approximation [27]. Eq. 4.1 implies that not the number of states, but the ratio of the particle and antiparticle densities of the state with the highest baryon number gives the biggest constrain on μ_B. The observed influence on the hadron densities can be seen as equal in all three cases for particles and antiparticles since the differences are negligibly small. Hence, a vanishing μ_B, which corresponds to equal production of particles and antiparticles, is obtained for the

4.3 Comparison to exponential growing spectrum

In the last part, the modified mass spectra spectra are compared to an exponentially growing spectrum, the asymptotic form of the Hagedorn proposal from section 1.4. The mass spectra are shown as histograms with a bin size of 200 MeV/c^2. The masses and temperatures in the histograms are given in natural units, where the speed of light and the Boltzmann constant are set to unity. The states are counted according to their degeneracy due to total angular momentum and isospin. The $\Delta(1232)$ resonance, for example, carries a total angular momentum of $J = \frac{3}{2}$, which corresponds to a degeneracy of $g_J = 4$. The total isospin of this state is $I = \frac{3}{2}$, leading to a degeneracy due to isospin of $g_I = 4$. Counting the $\Delta(1232)$ resonance adds therefore a total of 16 states to the mass bin from 1200 to 1400 MeV, four states with different third components of J for each of the four different third components of I.

Fig. 4.10 shows the GWU-modified PDG 2014 mass spectrum in the range from 0 to 4 GeV/c^2. For comparison, exponential functions of the form

$$\rho(m) \propto \frac{1}{kT} \cdot e^{\frac{m}{kT}} \tag{4.2}$$

are also shown in the figure, one for $kT = 200$ MeV, 250 MeV and 350 MeV, in the range from 0 to 2 GeV/c^2. For lower masses up to 2 GeV/c^2, the histogram seems to favour a temperature of 350 MeV, more than twice the temperatures obtained from the fits. This deviation arises from the validity region of the approximation.
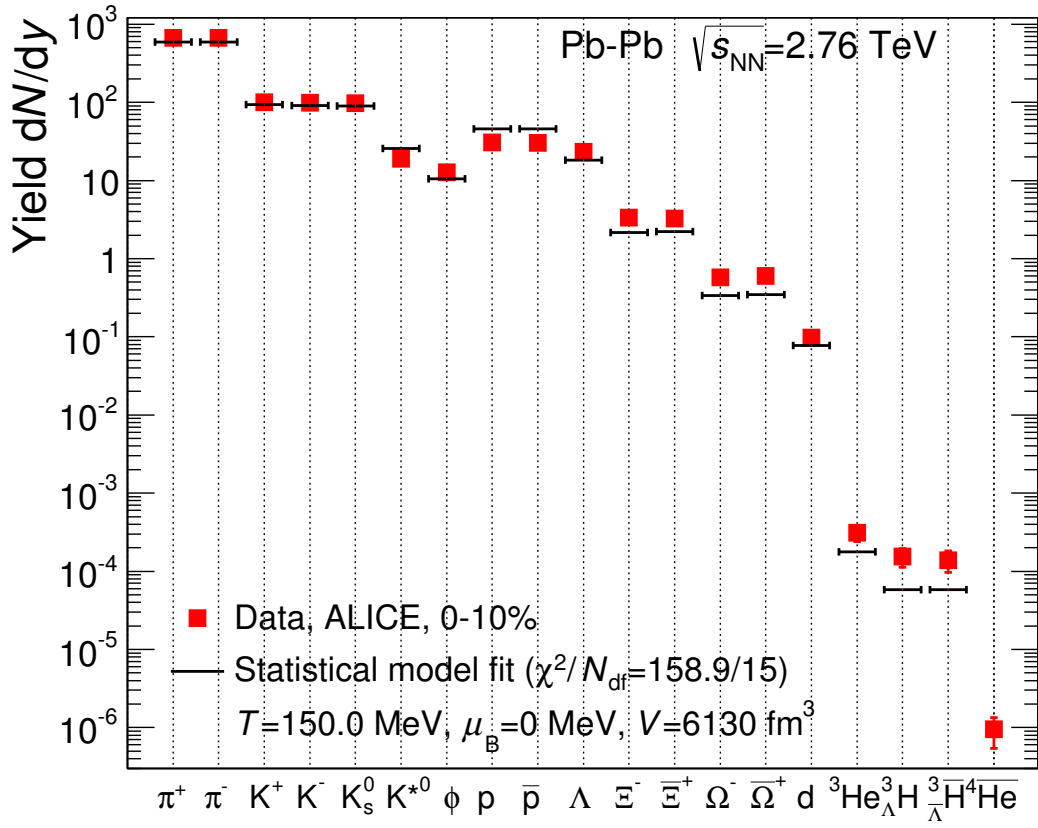
Figure 4.8: Extraction of T_{ch} and μ_B from fit on yields for spectrum of PDG 2014 with LQCD states.
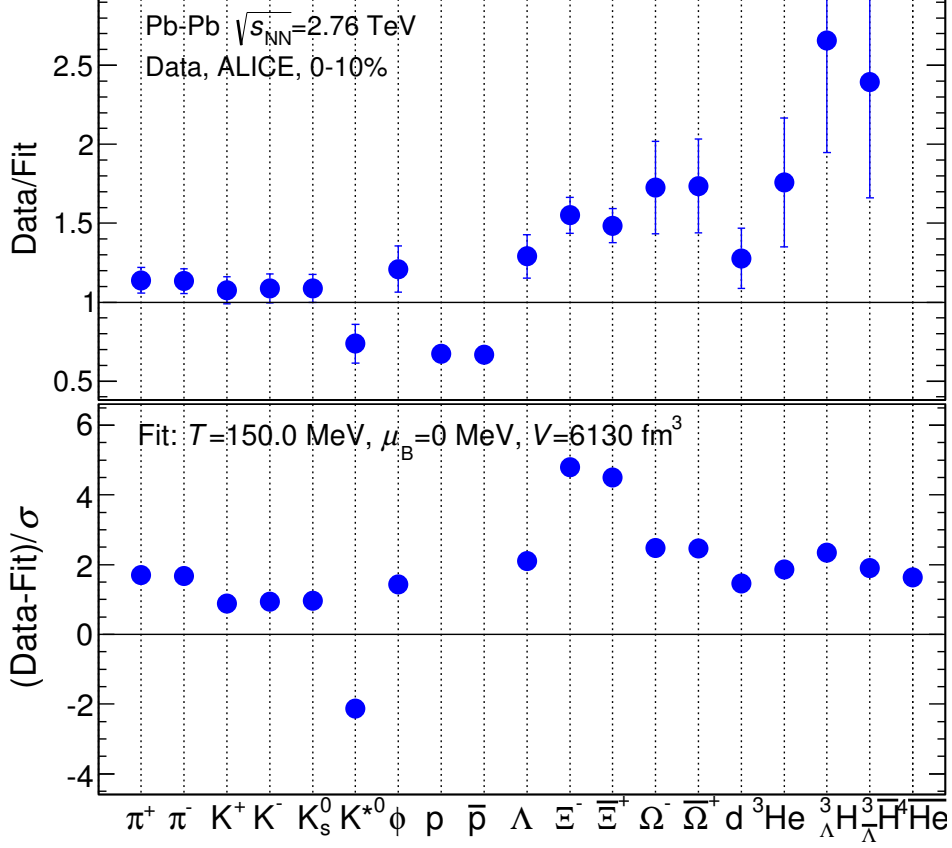
Figure 4.9: Differences between data and fit for the spectrum of PDG 2014 with LQCD.

The exponential functions are only approximations of equation 1.13, which is an approximation for large masses itself [20]. For lower masses, the $\frac{1}{m^a}$ factor is expected to become more dominating than the exponential factor. Therefore, if the spectrum has the form of Eq. 1.13, the number of states in the lower mass region should be smaller than the exponential function. This effect, although very small, can be seen for the curve of $kT = 350$ MeV. For smaller temperatures, the opposite effect can be seen in the figures.

Furthermore, the temperatures from the fits represent the system at chemical freeze-out, whereas the Hagedorn temperature signals the phase transition. These two temperatures do not necessarily need to coincide, as discussed in Section 1.2. For the higher mass region above 2 GeV/c^2, the exponential functions, due to their monotonous behaviour, continue to rise, whereas the mass spectrum shows a decreasing number of states for the higher mass region. The deviation can be explained by the experimental challenge of measuring these states. The spectra mostly rely on experimental information collected by the PDG. The higher the mass of a particle or resonance, the more difficult its identification becomes. And therefore the chance of finding evidence for such a state decreases with its mass.
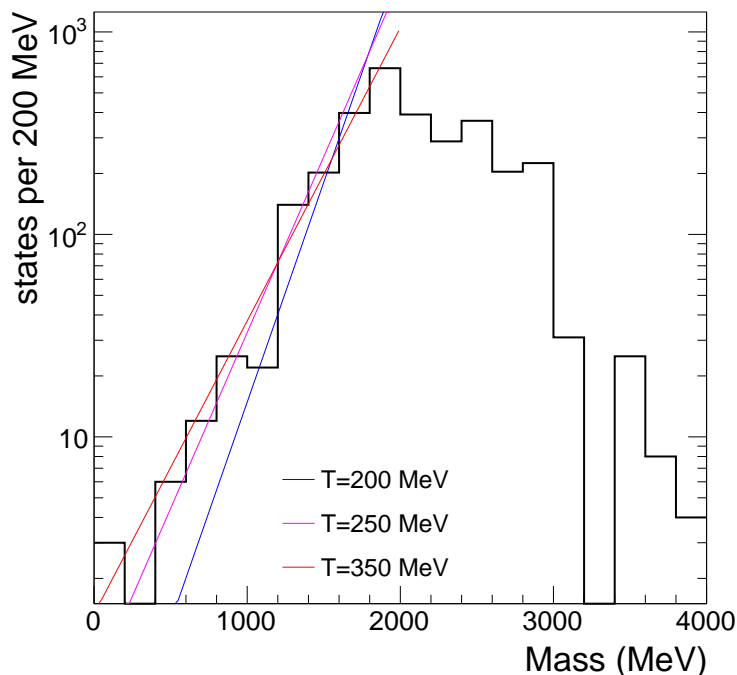
Figure 4.10: A histogram of the GWU-modified PDG 2014 mass spectrum. Approximated Hagedorn spectra for three phase transition temperatures are shown for masses up to 2 GeV/c^2.

An analogous plot for the unmodified PDG 2014 spectrum can be seen in Fig. 4.11. The histogram looks very similar to the first one. Again, for low masses, the temperature of 350 MeV seems to approximate the histogram best. In the moderate mass range, from 1.2 to 2 GeV/c^2, however, the purple curve seems slightly closer to the spectrum, corresponding to a temperature of 250 MeV. The additional states, 10 of which are in this mass range, can be taken as an explanation. Again, the highly approximative character of these exponential functions should be kept in mind when discussing their temperatures.

The spectrum of the PDG 2014 with LQCD states is shown in fig. 4.12. This spectrum exhibits an even broader peak, caused by the many additional states in the mass region between 1.2 and 2 GeV/c^2. Due to this increase, the exponential function corresponding to 250 MeV as critical temperature seems to be even more favoured than in the spectrum before. This reflects again the trend shown by the chemical freeze-out temperatures, where the lattice spectrum lead to the smallest temperature. The similarity of the spectra despite the many additions results from the logarithmic scale.
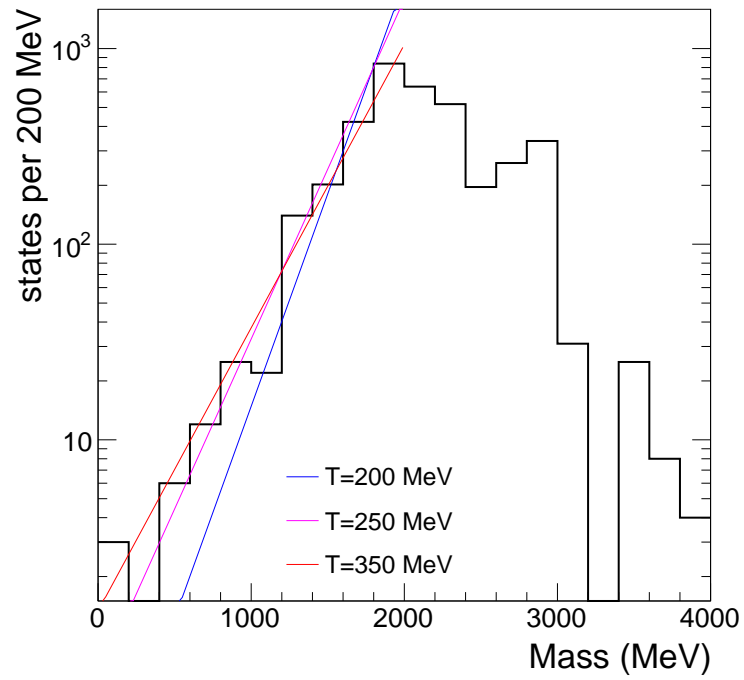
Figure 4.11: The unmodified PDG 2014 spectrum shows a broader peak and a different trend for the temperature than the first one.
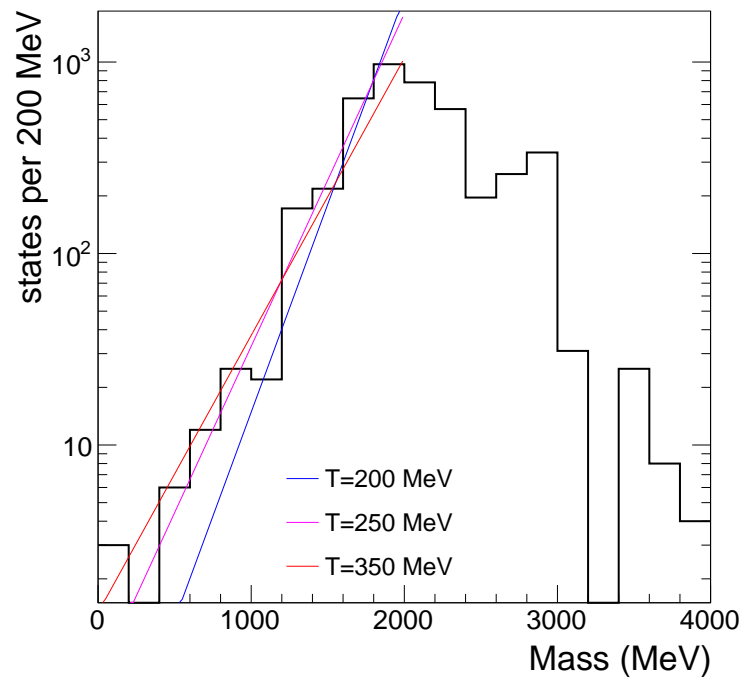

Figure 4.12: The PDG 2014 mass spectrum including the lattice states.

5 Conclusions

The influence of three different hadron spectra on the calculations of particle densities in the thermal model of heavy-ion collisions has been studied. The three spectra differ in their light flavour nonstrange baryon content. The chemical freeze-out temperature T_{ch} and the baryochemical potential μ_B have been determined through fits to hadron yields measured by the ALICE collaboration at the LHC. The spectra have also been compared to approximately exponential spectra as predicted by Hagedorn.

A dependence of final state hadron densities on the employed spectrum has been seen. Removing resonance states from the spectrum leads to a decrease in the densities of their decay products, mostly protons, neutrons and pions. Adding resonances has the opposite effect, increasing the densities due to additional feed-down from these states. When modifying the light flavour baryon sector, the relative influence on the baryon densities is much higher than on the meson densities. This is induced by a shift of balance between the meson and baryon sector. The addition of many theoretical baryon states, as has been done in the LQCD case, without adding the theoretical meson states in the same mass range, promotes creation of baryons because of additional phase space in comparison to the unmodified case.

By inverting this logic, if one were to accept the thermal model as universally valid and applicable despite the deviations for protons in these collisions, one could derive a test for the existence of theoretical states. If the inclusion of such a state were to improve fit qualities, one might have an indication for its existence, whereas a poorer fit quality might indicate its absence. But many further studies are needed to support or reject this rather strong conclusion. Therefore, no conclusions about the existence of the proposed lattice states can be made yet, as the modified spectra display an unphysical character. The chemical freeze-out temperature shows only a weak dependence on the spectrum. The three cases lead to temperatures $kT_{ch} = 157$ MeV for the first, $kT_{ch} = 156$ MeV for the second and $kT_{ch} = 150$ MeV for the third one. The addition of 51 resonance states leads to a drop in temperature of about 5%, implying a weak sensitivity to changes in and incompleteness of the spectrum. The removal of states shows an improvement of fit quality and a rise in temperature, whereas the addition again causes the opposite effects. This tendency, as it might be caused by the aforementioned imbalance, as well as the temperatures have to be treated with caution. But the amount of stability of the temperature to such unbalanced changes can be used for an estimation of the systematic uncertainties. A better estimate can be achieved by expanding this study to other hadron sectors to reduce the imbalance.

The baryochemical potential in all three cases is determined to be $\mu_B = 0$ MeV. A dependence on the spectrum has not been found. This is in agreement with expectations. The baryochemical potential μ_B, which describes the ratio of baryons and antibaryons, is not expected to depend on how many different baryon species are considered as intermediate states, but rather on the ratio of produced baryons and antibaryons. This ratio is compatible with unity at the LHC.

For the mass region up to 2 GeV/c^2, all three spectra show an approximately exponential dependence on the mass. No contradiction to a Hagedorn-like mass spectrum in this region has been found. The critical temperatures in natural units for the three scenarios in this approximation have been found to be of the order of 250 MeV. The mass region above 2 GeV/c^2 does not show exponential behaviour. Whether this is caused by states that have yet to be identified or by an actually non-exponential spectrum, cannot be concluded at this stage.

6 Outlook

The considered hadron spectrum has an ample influence on the calculable particle densities in the thermal model. The implementation of the most complete hadron spectrum is very important for an accurate description of particle yields when using thermal model methods. The inclusion of theoretical states has to be done with caution in order to prevent an imbalance between different sections of the hadron mass spectrum. To further study the influence and to better estimate the uncertainties due to an incomplete hadron spectrum, equal studies such as this one in every domain of the spectrum need to be conducted. Already, lattice results for the strange baryon sector by the same group are available, as well as for the isoscalar [28] meson and charmed [29] baryon sector. Due to the strong increase in computing power and the constantly improving numerical methods, the results from lattice QCD are expected to become more reliable and precise. And with the data from RUN2 of the LHC, changes in the experimental results for particle yields and information on additional states can also be expected. Thermal model calculations might lead, in the end, to a test for these spectra. This underlines its crucial role in the phenomenology of heavy-ion collisions.

Bibliography

[1] G. Aad et al. Observation of a new particle in the search for the Standard Model Higgs boson with the ATLAS detector at the LHC. *Phys. Lett.*, B716:1–29, 2012.

[2] S. Chatrchyan et al. Observation of a new boson at a mass of 125 GeV with the CMS experiment at the LHC. *Phys. Lett.*, B716:30–61, 2012.

[3] M. D. Thomson. *Modern particle physics*. Cambridge University Press, Cambridge [u.a.], 2013.

[4] J. Stachel, A. Andronic, P. Braun-Munzinger, and K. Redlich. Confronting LHC data with the statistical hadronization model. *J. Phys. Conf. Ser.*, 509:012019, 2014.

[5] P. Braun-Munzinger, K. Redlich, and J. Stachel. Particle production in heavy ion collisions. *Invited Review for Quark Gluon Plasma 3*, 2003.

[6] A. Andronic, P. Braun-Munzinger, K. Redlich, and J. Stachel. The statistical model in Pb-Pb collisions at the LHC. *Nucl. Phys.*, A904-905:535c–538c, 2013.

[7] Betty Abelev et al. Pion, Kaon, and Proton Production in Central Pb–Pb Collisions at $\sqrt{s\_NN} = 2.76$ TeV. *Phys. Rev. Lett.*, 109:252301, 2012.

[8] G. F. Sterman. Quantum chromodynamics. *Encyclopedia of Mathematical Physics*.

[9] S. Bethke. Experimental tests of asymptotic freedom. *Prog. Part. Nucl. Phys.*, 58:351–386, 2006.

[10] P. Braun-Munzinger and J. Wambach. The Phase Diagram of Strongly-Interacting Matter. *Rev. Mod. Phys.*, 81:1031–1050, 2009.

[11] D.H. Rischke. The Quark gluon plasma in equilibrium. *Prog. Part. Nucl. Phys.*, 52:197–296, 2004.

[12] S. Gale, C.and Jeon and B. Schenke. Hydrodynamic Modeling of Heavy-Ion Collisions. *Int. J. Mod. Phys.*, A28:1340011, 2013.

[13] P. Braun-Munzinger, J. Stachel, and Christof Wetterich. Chemical freezeout and the QCD phase transition temperature. *Phys. Lett.*, B596:61–69, 2004.

[14] C. Blume. Is there Life after Hadronization? An Experimental Overview. *Acta Phys. Polon.*, B43:577–586, 2012.

[15] A. Bazavov et al. Equation of state in (2+1)-flavor QCD. *Phys. Rev.*, D90(9):094503, 2014.

[16] S. Borsanyi, Z. Fodor, C. Hoelbling, S. D. Katz, S. Krieg, and K. K. Szabo. Full result for the QCD equation of state with 2+1 flavors. *Phys. Lett.*, B730:99–104, 2014.

[17] P. Braun-Munzinger and J. Stachel. The quest for the quark-gluon plasma. *Nature*, 448(7151):302–309, July 2007.

[18] F. Schwabl. *Statistische Mechanik*. Springer-Lehrbuch. Springer, Berlin ; Heidelberg [u.a.], 3., aktualisierte aufl. edition, 2006.

[19] A. Tounsi and K. Redlich. Strangeness enhancement and canonical suppression. hep-ph/0111159. 2001.

[20] R. Hagedorn. How we got to qcd matter from the hadron side by trial and error. *Invited talk at "Quark Matter 1984", Fourth International Conference on Ultra-Relativistic Nucleus-Nucleus Collisions, Helsinki*, pages 53–76, 1984.

[21] R. Dashen and H. J. Ma, S.-k.and Bernstein. *s*-matrix formulation of statistical mechanics. *Phys. Rev.*, 187:345–370, Nov 1969.

[22] A. Andronic, P. Braun-Munzinger, J. Stachel, and M. Winn. Interacting hadron resonance gas meets lattice QCD. *Phys. Lett.*, B718:80–85, 2012.

[23] K.r Zalewski and K. Redlich. Thermodynamics of the low density excluded volume hadron gas. arxiv:1507.05433. 2015.

[24] A. Andronic, P. Braun-Munzinger, and J. Stachel. Hadron production in central nucleus-nucleus collisions at chemical freeze-out. *Nucl. Phys.*, A772:167–199, 2006.

[25] K. A. Olive et al. Review of Particle Physics. *Chin. Phys.*, C38:090001, 2014.

[26] R. G. Edwards, J. J. Dudek, D. G. Richards, and S. J. Wallace. Excited state baryon spectroscopy from lattice QCD. *Phys. Rev.*, D84:074508, 2011.

[27] I. Heppe. Ein statistisches modell für die teilchenproduktion in hochenergetischen schwerionenkollisionen. Diplomarbeit, Heidelberg, 1998.

[28] J. J. Dudek, R. G. Edwards, P. Guo, and C. E. Thomas. Toward the excited isoscalar meson spectrum from lattice QCD. *Phys. Rev.*, D88(9):094505, 2013.

[29] P. Madanagopalan, R. G. Edwards, and M. J. Mathur, N.and Peardon. Spectroscopy of charmed baryons from lattice QCD. *PoS*, LATTICE2014:084, 2015.

Acknowledgements

First of all, I would like to thank Prof. Dr. Johanna Stachel for letting me be a part of the ALICE group and for the many interesting discussions on my work.

I also would like to express my deep gratitude to Michael Winn, for putting up with my daily questions and providing support and knowledge when needed, even in the middle of the night. And, of course, for the proofreading of this thesis.

I would also like to thank Dr. Anton Andronic for providing thermal codes and ROOT macros, and a few fruitful visits at the GSI.

Furthermore, I would like to thank Prof. Dr. Klaus Reygers for evaluating my thesis.

Lastly, I would like to extend deep gratitude to my friends and family for supporting me during these last months.

Eidesstattliche Erklärung

Ich versichere, dass ich diese Arbeit selbstständig verfasst und keine anderen als die angegebenen Quellen und Hilfsmittel benutzt habe.

Heidelberg, den 19. August 2015   Unterschrift: _____